High Voltage

Research Article

IET Journals
The Institution of Engineering and Technology

Comparative characterisation of conventional and textured 11 kV insulators using the rotating wheel dip test

eISSN 2397-7264
Received on 26th July 2019
Revised 14th April 2020
Accepted on 26th April 2020
E-First on 22nd June 2020
doi: 10.1049/hve.2019.0189
www.ietdl.org

Adnan Krzma[1,2] ✉, Maurizio Albano[1], Abderrahmane Haddad[1]

[1]*Advanced High Voltage Engineering Research Centre, School of Engineering, Cardiff University, Wales, UK*
[2]*Department of Electrical and Computer Engineering, Faculty of Engineering, Elmergib University, Al-Khom, Libya*
✉ *E-mail: Krzmaa@cardiff.ac.uk*

Abstract: Surface tracking and erosion is an irreversible degradation occurring on the insulator surface, and this can ultimately lead to failure of the insulator. Polymeric materials such as silicone rubber have many advantages; including a superior hydrophobic surface. However, polymers are exposed to ageing and degradation resulting from electrical and environmental stresses. The rotating wheel dip test is adopted to conduct a comparative study of surface conduction on the two insulators. A conventional design has been selected and compared with insulators having textured surface. Monitoring of the shed surface and insulator trunk using an IR camera were carried out to assess the temperature distribution along insulator profiles. A spatial analysis was also performed to identify key features of the two designs. Localised surface conductance measurements are proposed in this study. This helps to understand and distinguish the trends of conductance and its distribution on each surface, helping to predict the future surface degradation associated to each design.

1 Introduction

Silicone rubber (SiR) polymeric insulators have now gained a great acceptance and are widely used in the overhead power distribution and transmission lines. This growth of use is attributed to inherent promising advantages over conventional porcelain and glass insulators [1, 2]. One of the most important properties of SiR insulators is hydrophobicity, which is defined as the ability of polymeric materials to repel water on their surfaces. SiR insulators are considered to have good hydrophobic properties and, so, have an excellent pollution flashover performance compared to that of traditional hydrophilic insulators made from porcelain and glass [3, 4].

On surfaces of the ceramic high voltage insulators, water readily forms a continuous film on the hydrophilic surface. In the presence of contamination, a leakage current develops, which may ultimately lead to flashover of the insulator. The hydrophobic surface properties of SiR insulators prevent the formation of a continuous film, and the water remains as individual droplets, which may simply flow away from the surface [5, 6].

Pollution flashover can be mitigated by improving both insulator design and material properties [7, 8]. Ceramic insulators are made from an arc resistant material with high internal strength and excellent immunity to ultraviolet (UV) radiation. For ceramic insulators, the prevailing factor of pollution performance is leakage distance, where high leakage distance improves performance [9]. SiR polymeric insulators are not arc resistant as ceramic insulators and are influenced by UV radiation. However, better pollution performance, reduced breakage and high flexibility make them an attractive option when selecting insulators for outdoor applications [10].

As SiR insulators can be sensitive to outdoor climate conditions, it is crucial to evaluate their long-term performance under different environmental conditions [11, 12]. The available literature review has shown that the electrical performance of SiR insulators is correlated to their surface properties. The surface situation of SiR insulators that are operated in severe environment conditions has been found to worsen with age. Ageing has been found to reduce the overall electrical performance of polluted SiR insulators and cause an increased incidence of discharge activities and dry band arcing on the surface. This increase can degrade the housing material by tracking and/or erosion, which in severe cases, leads to damage to the insulator [13]. Therefore, the surface degradation and insulator flashover due to these discharges is still a subject of concern.

Harsh environmental conditions would still result in discharge activities on the insulator surface, and the design of SiR insulators remains very simple due to the moulding limitations, which prevent the development of complex insulator profiles [14].

Textured insulators are a novel approach [15] to the design of polymeric insulators and have brought many advantages to improving insulator performance. Various textured designs of the polymeric surface may be achieved by using a pattern comprising an array of contiguous or overlapping protuberances. The aim of this design is to reduce the power dissipation by reducing both the electric field strength and the current density in the shank regions. This may be managed by increasing both the surface area and the creepage distance of the insulator without increasing its overall longitudinal length [14].

Furthermore, it is observed that compared with conventional samples, textured patterns might mitigate the damage induced on polymeric materials due to surface discharges by presenting multiple paths for current conduction: when one current path initiates drying as a result of Joule heating, its resistance will increase. At this instant, the current flow will shift to a different path of lower resistance before significant thermal degradation occurs.

This paper presents the details for the experimental setup, the insulator preparation, the mechanical design, the software and hardware computer tools and the measurement techniques used. Moreover, the performance of two different designs of SiR insulators textured and non-textured were investigated and compared.

2 Insulator preparation

Different types of four-shed insulator designs were used in this study, which were manufactured within the Cardiff HV laboratory facilities using room-temperature vulcanised (RTV-2) two-component SiR (600A/B) and by casting over a glass-fibre core with aluminium end fittings crimped at each end. The mechanical and electrical properties of the 600A/B liquid silicone used in this work are given in Table 1. The pigtail and pin aluminium fittings were attached directly to the fibreglass core, as illustrated in Fig. 1.

Table 1 Characteristics of 600 A/B SiR materials [16]

Property	Inspection method	600 A/B
permittivity	IEC 60250	2.9
dielectric strength, kV/mm	IEC 60243	23
tracking resistance	IEC 60587	1A 3.5
dissipation factor	IEC 60250	3×10^{-4}
tensile strength, N/mm^2	ISO 37	6.50
hardness shore	ISO 868	30
tear strength, N/mm	ASTM D 624 B	20
elongation at break	ISO 37	500
volume resistivity	IEC 60093	10^{15}

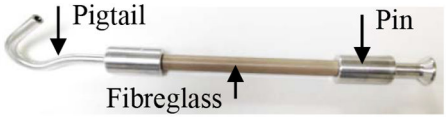

Fig. 1 *Pigtail and pin aluminium end fitting design*

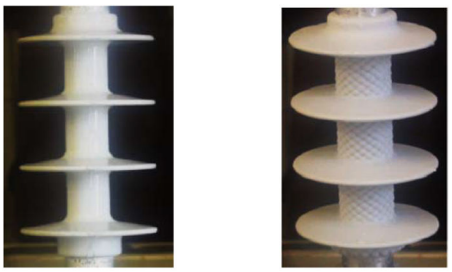

Fig. 2 *Test samples for RWDT system*
(a) Conventional insulator, ***(b)*** Textured-trunk insulator

Table 2 Dimensions of tested insulators

Parameters	Conventional (CONV), mm	Textured (TT6), mm
creepage distance	375	471
fitting separation	175	175
shed diameter	90	90
shed separation	46	46
trunk diameter	28	28
inner core diameter	18	18
form factor	2.7	2.7

A superior adhering primer was used to enhance the adherence of the SiR to the metal surfaces of the pin and the pigtail. Strong bonding between them was achieved and verified with laboratory tests.

The insulator profile adopted was based on a conventional design (CONV), as shown in Fig. 2*a*. The same basic profile was used for the textured insulators. The textured surface having texture hemispheres of 6 mm diameter were moulded on the insulator trunk (TT6) (Fig. 2*b*). The dimensions of both insulator designs are summarised in Table 2. Both two types of SiR insulators were fabricated in the High Voltage Laboratory at Cardiff University. The conventional insulator was manufactured as a standard commercial insulator available on the market, while the TT6 insulator was designed based on the same basic profile of a standard insulator with added textured surface enhancement of the insulator trunk. The RTV-2 silicone material was prepared by mixing two components: base resin (600A) and the curative (600B) with a ratio of 9:1 using an MCP 5/01 vacuum casting machine (Fig. 3*a*). During the casting process, the mixed components were injected into the mould.

As can be seen in Fig. 3*a*, the main components of the casting machine are (1) the top mixing chamber, (2) the lower injection chamber and (3) the touch control panel. The mixed components of SiR (600A/B) are placed in the top chamber while the mould is placed in the lower chamber.

At the beginning of the casting process, trapped air is removed from the mixed components by degassing the top chamber for a few minutes. After about 12 min of degassing and mixing, the SiR component is ready to be injected into the lower part of the casting machine where the mould is located. During the injection process and due to the complex geometry of the mould, a variable pressure is applied to force the mixture to fill the mould cavity. When the materials start to emerge from venting channels, the mould cavity becomes full. The vacuum casting machine is then switched off and the mould placed on the oven for curing at 50°C for 8 h. Next, the mould is left to cool for 1 h, before the mould is separated to reveal the cast (Figs. 3*b* and *c*). The insulator is then removed from the mould and visually inspected for any visible defect or void. If no imperfection appears, it is left for an extra 24 h at room temperature to ensure that the cross-linking of the polymer has been completed [17].

3 RWDT design and construction

A rotating wheel dip tester was designed and constructed in accordance with IEC 62730 standards [18]. The apparatus was designed to be able to accept AC and DC voltages. Figs. 4 and 5 show the circuit diagram and the arrangement setup of the RWDT test.

The Ferranti high voltage 7.5 kVA, 100 kV step-up transformer was fed from the 230 V mains supply voltage through a voltage controller, an isolating transformer and a low-pass LC filter. For DC tests, the Glassman WX15P70 Series DC source was utilised to provide 1 kW of output power with a voltage up to 15 kV and a current of 70 mA. A 2 rpm DC permanent magnet motor with a single pole single throw normally open relay was used to attain the rotational movement of the test insulators. The tank used for the salt solution was made of a glass reinforced plastic material with dimensions of 1.6 m × 0.25 m × 0.75 m.

The voltage and current transducers consisted, respectively, of a capacitive voltage divider with a ratio of 3750:1 and a 200 Ω shunt resistor with low inductance for current measurement. The voltage and current signals were acquired using a computerised data acquisition system. For this purpose, a data acquisition (DAQ) card (MIO-16E series) was used, and its input was protected using a three-stage overvoltage protection system.

3.1 Experimental conditions

Based on IEC 62730:2012 standard, the applied voltage during the test under alternating and direct excitations should be 35 V/mm multiplied by the leakage distance. The leakage distance of the tested conventional insulator was calculated as 375 mm. The salinity of the solution in the test tank, consisting of NaCl and deionised water, was 1.4 g/l, and the salt solution shall be replaced weekly.

During the test, each revolution of rotation should have four test positions consisting of energisation, de-energisation, dipping and dripping positions. The test samples of the same design shall be evaluated together. Pairs of test samples of different design shall be assessed separately. To successfully meet the acceptance criteria and pass the tracking wheel test, the surface tracking and erosion should not reach the glass fibre core and puncturing of the shed or housing was not allowed.

3.2 Experimental procedure

Before starting the test, the insulators were cleaned with deionised water and then mounted in the wheel test ring as shown in Fig. 6. In this test, each revolution takes 192 s with four test positions consisting of energisation, cooling, dipping and dripping. For each position, the test sample remains stationary for about 40 s, and it takes 8 s to rotate through 90° from one position to the next. In the first position, the insulator is dipped into the saltwater. The second position of the cycle allows the excess saline solution to drip off from the sample, ensuring the formation of a thin wet layer on the surface. In the third position, the sample is subjected to high

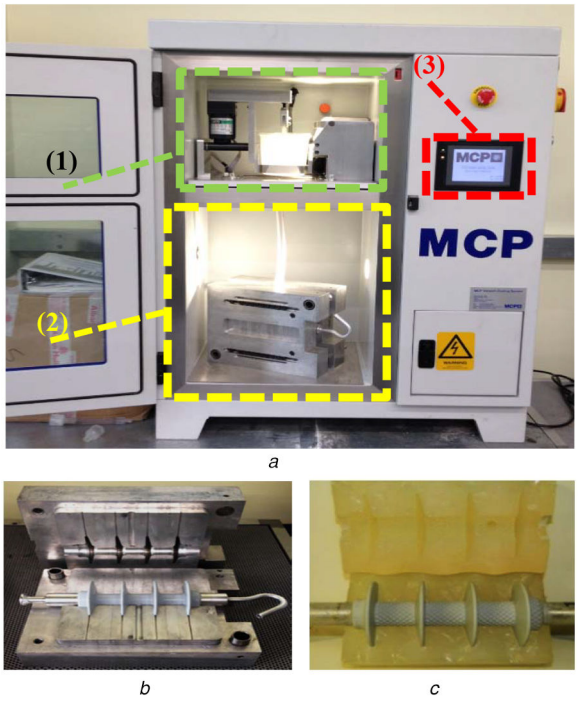

Fig. 3 *Casting process for SiR outdoor insulators*
(a) Vacuum casting machine: (1) the top mixing chamber, (2) the lower injection chamber, (3) touch control panel, ***(b)*** Conventional insulator, ***(c)*** Textured insulator

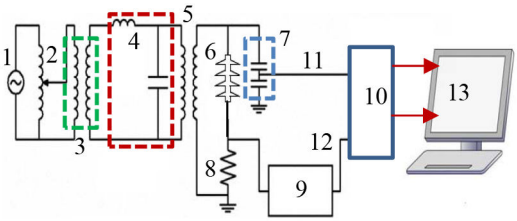

(1) 220V/main supply (8) 200 Ω resistor
(2) Variac (9) Protection system
(3) Isolating transformer (10) DAQ card
(4) (L-C) Filter (11) Voltage signal
(5) 100kV step-up transformer (12) LC signal
(6) SiR insulator (13) PC
(7) Voltage divider

Fig. 4 *Circuit diagram of RWDT system*

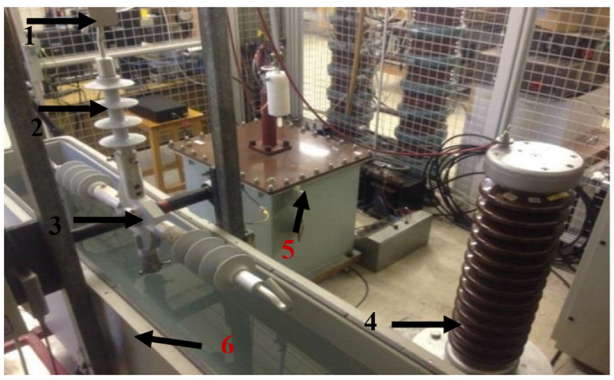

(1) HV electrode (2) SiR insulator
(3) Aluminium wheel (4) Voltage divider
(5) Step-up transformer (6) GRP tank

Fig. 5 *Test set-up of RWDT on 11 kV polymeric insulator*

voltage energisation. In the last stage of the test revolution, the surface of the tested insulator, which had been heated by discharges activities and dry band arcing in the previous period, is allowed to cool down [18].

3.3 Electric circuit of RWDT

As can be seen on Fig. 5, a metal frame is used to hold the wheel tester. At the top of this frame, a non-conductive bar is placed to support the electrode that was used to energise the insulator. In this circuit, the electrode is made of aluminium with some movement of the bar allowed to ensure good contact with the insulator at this position. The ground terminal of the insulator is electrically attached to the aluminium wheel; the wheel is then connected to the ring placed at the end of the rod through a cable that passes into a groove made in the rod. The ring then contacts a carbon brush, which is pressed against the ring during the revolution using a spring located behind it to ensure good contact. The brush is connected to a 200 Ω resistor, which is grounded and placed in a metal box equipped with a BNC connector and an overvoltage protection circuit [18]. The voltage signal across this resistor is acquired by the DAQ card through a coaxial cable (RG58). The signal is then saved into a personal computer using a LabVIEW code. The operating voltage signal is acquired directly to the DAQ system through a capacitive voltage divider and a BNC attenuator with a total ratio of 3750:1.

For the motor control system, the speed regulator and a box in which the relay is housed are placed on the other side of the frame. The relay receives the control signal from a digital output pulse generated by the DAQ card and the LabVIEW routine. The complete cell is firmly fixed to the metal frame equipped with wheels, which allow it to be easily moved.

3.4 Motor and drive control

In order to move the wheel where the insulator is mounted, a DC permanent magnet motor was used. Choosing such a kind of motor provides simple speed control and offers a fast response to starting and stopping. The requirement to have a simple speed control is due to the different weights of insulators; each type of insulator requires different torques to achieve the same movement time (8 s) between two different positions. As the torque/speed characteristic of a DC motor is quite linear, the speed can be simply controlled by changing the current [19].

Using the LabVIEW graphics programming language [20], an appropriate code was written to control the motor of the RWDT. The program was developed to control the motor speed and rotate the motor in the desired position. To generate the input signal for stopping the motor, it was decided to use the value of the instantaneous power as a threshold condition [21]. Thus, when the insulator touches the high voltage electrode, the instantaneous power value reaches the threshold level. At this same time, the DAQ card generates a digital output signal to stop the motor. In this way, the user can follow the number of cycles that are run during the test and determine the optimal threshold value required to stop the motor. Fig. 7 shows the flow chart of the motor control program and how it communicates with the main data acquisition system. The data acquisition and the motor control programs were linked together to detect the number of cycles completed during the test. The program stages to achieve this interfacing are described as follows:

(a) The global variable value of the instantaneous power is created to interface both programs, and through this value, it is possible to check whether the motor has to be stopped.
(b) When the insulator rotates between the two positions, the program outputs a digital pulse of 5 V, and the average power value is under the threshold level.
(c) While the insulator is in a vertical position, where it is energised, the average power value exceeds the threshold level and the digital output of the program is carried down at 0 V, thus driving the motor to stop.
(d) Once the motor has stopped, the global variable of the average power is set to true, thus allowing the DAQ system to run. After

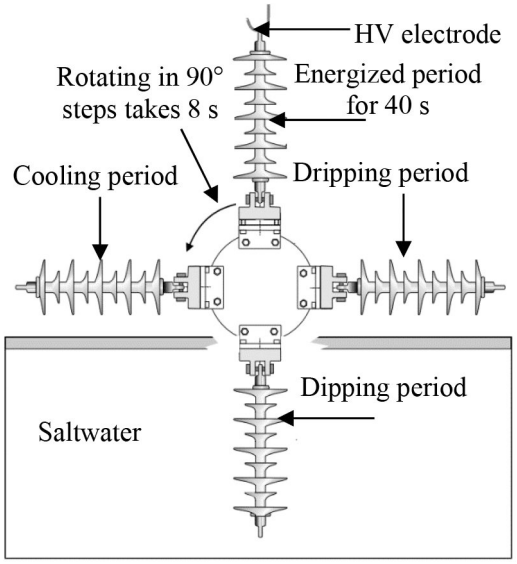

Fig. 6 *Schematic diagram of the RWDT [18]*

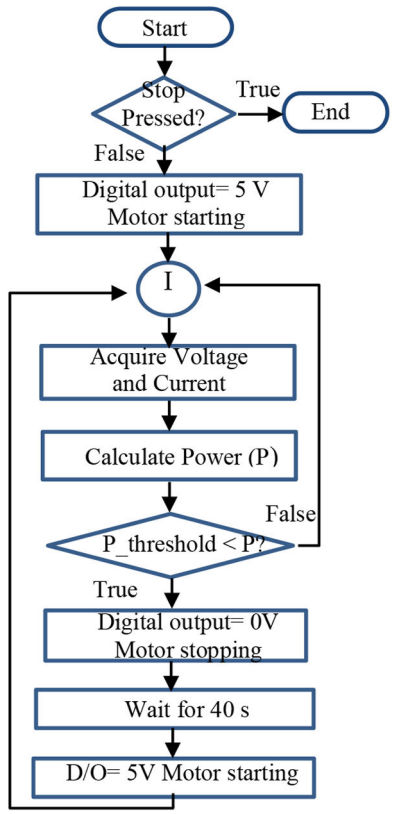

Fig. 7 *Flow chart of the motor control program*

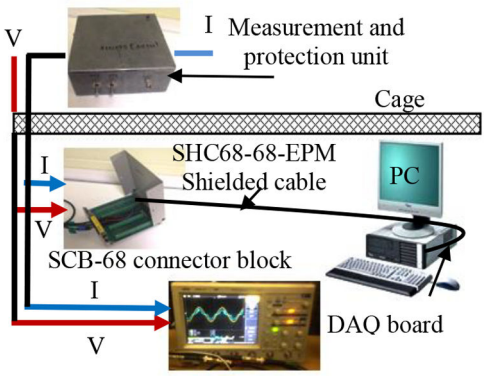

Fig. 8 *Arrangement of data acquisition system*

40 s, a pulse of 5 V is sent again to activate the motor and rotate the insulator to the next position.

An additional improvement is the implementation of an optical incremental encoder to control the rotational speed and to achieve very good precision on vertical alignment with a wide range of insulator design and weights.

The AEDB-9140 series encoder is three-channel optical incremental module. Each module consists of an LED source and a detector enclosed in a small plastic package. The AEDP-9140 encoder has two-channel quadrature outputs and the third channel is an index output. This index output is a 90 electrical degree high true pulse which is generated once for each full rotation. The AEDP-9140 provides sophisticated motion control detection at low cost, making them an ideal option for different applications [22].

3.5 Data acquisition system

The E-series MIO-16E National Instruments board was used to acquire the leakage current and the voltage signals during the tests. The maximum input range varied between −10 and +10 V. The data acquisition board can acquire either 32 single-ended analogue inputs or 16 differential analogue inputs. The physical connection between the board and the RWDT control unit was attained by an SCB-68 connector block, as illustrated in Fig. 8. The connection between the connector and the DAQ board was made with an SHC68-68-EPM shielded cable. The data acquisition (DAQ) program of the RWDT was also built in LabVIEW. The program was designed to acquire, monitor and store the waveforms of leakage current and applied voltage signals. The interface of the DAQ program with the motor control system is achieved.

The DAQ software starts acquiring/saving data when the insulator makes contacts with the HV electrode. The sample rate of the data acquisition board is 10^4 samples/s for each of the two analogue channels of the voltage and current signals. The leakage current and voltage traces were stored in a Technical Data Management Streaming (TDMS) file format [23]. Data were saved in sets of 200 samples, which represent one cycle of the 50 Hz voltage and current waveforms. The acquisition of samples was repeated until all 4×10^5 samples had been processed and, then, the next file was accessed. Each acquired file represented the saved data of one-wheel revolution.

3.6 Post-processing data

The post-processing LabVIEW program was developed to read and analyse the data acquired from the RWDT. The program allows the user to choose the path from which to read the saved files and determines a specific path for the calculated parameters. The code is also responsible for specifying the electrical characteristics to be analysed. The electrical parameters, such as the peak and root mean square (rms) leakage current of the applied voltage, average power dissipation, power factor angle and absorbed energy are calculated. Studying the behaviour of these parameters helps to evaluate the performance of SiR insulators and material degradation under test conditions. The rms leakage current magnitude is used to evaluate the behaviour of discharge activity that occurred on the insulator surface. These discharges may lead to surface drying and, ultimately, the formation of dry bands on the surface. The average power dissipation is used to measure the heat dissipated on the surface of the insulator since it is one of the major causes of material degradation. The cumulative dissipated energy is used to calculate the total energy absorbed on the insulator surface and based on these losses, the degradation level on the surface can be estimated. The power factor index calculates the phase shift angle between the voltage and the leakage current, which can be used to distinguish the features of the resistive surface conduction and surface discharge activity.

4 Thermal and visual cameras records

The visual and thermal observations of discharge activities and dry band formation on the surface of tested insulators during the wheel

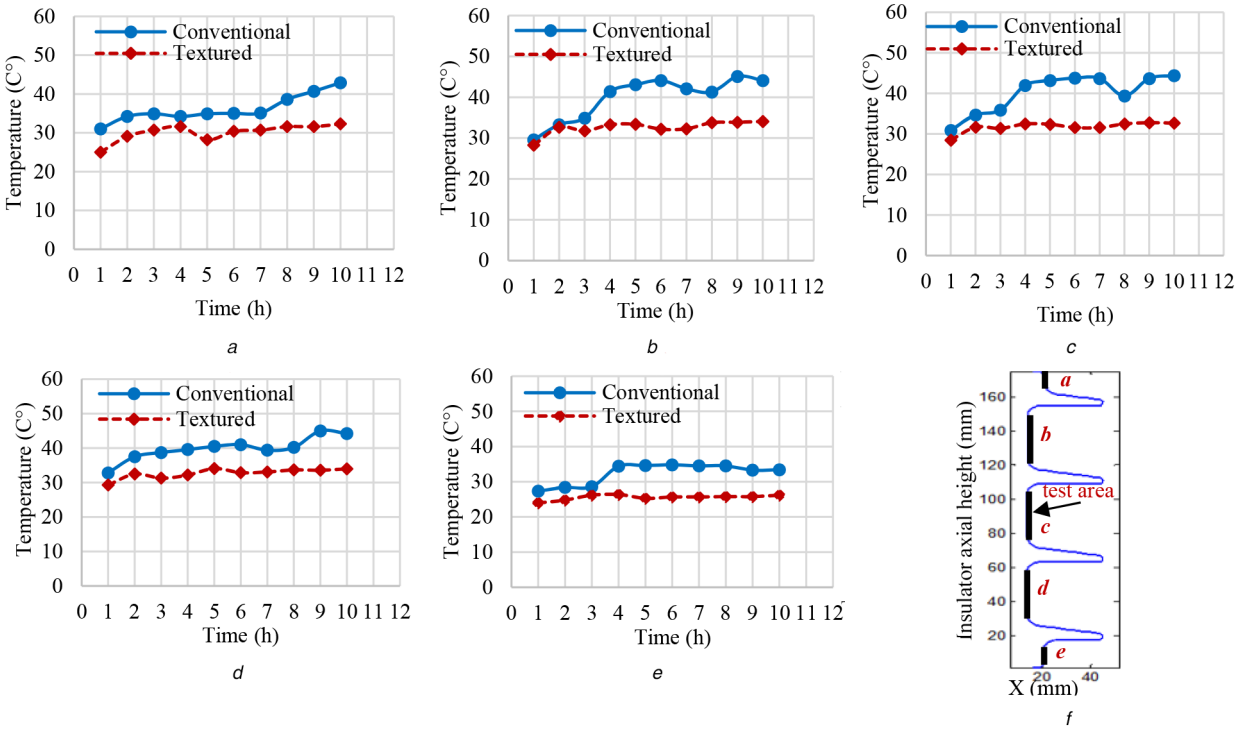

Fig. 9 *Temperature distribution along the surface profiles of conventional and textured insulators during the RWDT*
(a) Trunk A, ***(b)*** Trunk 1, ***(c)*** Trunk 2, ***(d)*** Trunk 3, ***(e)*** Trunk B, ***(f)*** Insulator profile

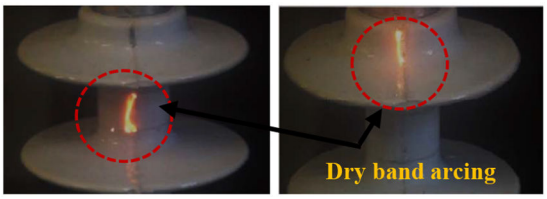

Fig. 10 *Discharges activities during RWDT*

Fig. 11 *Visual image of tested conventional insulator*

tests were performed using a FLIR A325 infrared (IR) thermal camera and a high-resolution video camcorder. The purpose of the IR imaging is to reveal any surface heating due to discharge activity and to detect dry band formation that may occur during the test, while the video camera was used to capture any discharge activity. The calibration of the IR camera was performed using an insulator at a known temperature. The calibration performance by the manufacturer in a recent maintenance service also confirms the precision of the device within ±0.2°C from the target temperature.

Using the FLIR ThermaCAM Research software, the camera saves the IR records as SEQ files. The IR camera has a spectrum range from 7.5 to 13 µm with an IR resolution of 320 × 240 pixels and an image frequency up to 60 Hz. Both the IR thermal and video cameras were fixed on tripods and placed outside the rotating wheel dip tester. Fig. 9 shows the temperature distributions along the surface profiles of conventional and textured insulators.

During the 10 h wheel test, the temperature distribution along the trunk regions (trunk A, trunk 1, trunk 2, trunk 3 and trunk B) of tested insulators was measured. It can be clearly observed from the graphs that a higher temperature value was recorded on the conventional insulator. This is attributed to the higher discharge activity and dry band arcing occurring on this surface, which is not observed on the textured insulator during the energisation period.

The visual capture recorded by the digital camera reveals visible discharge activity and dry band arcing on the trunk surface of the conventional insulator. As illustrated in Fig. 10, the yellowish light of dry band arcing can be seen. Such arcing leads to tracking on the SiR surface [24].

After the end of the wheel test, significant changes in the tested sample surfaces were observed. Surface degradation by tracking and erosion was detected. Fig. 11 shows surface tracking on the moulding line of the conventional insulator trunk close to both energised and ground ends. Occurring of such tracking on the moulding seam can cause irreversible damage to polymeric insulators under severe pollution conditions [25, 26].

Further test data processing is performed using the MATLAB environment in order to gain a better understanding of a temporal variation during the test and to identify any possible location of higher stress on the insulator surface. The MATLAB analysis identifies the temperature value for each pixel of each selected area and create the distribution of the temperature clustering the data in a class of 2.5 C. This help to understand the temperature distribution over the area and the extension of the hot area. Figs. 12 and 13 show the comparison of the analysis of the frequency temperature distribution of a conventional and textured insulators. The two designs show a very different pattern with the second distribution is more uniform and with lower average temperature.

This spatial analysis helps to identify any improvement between designs. In this test, the presence of the seams due to the manufacturing process is evident in both designs. However, it impacts more consistently the smooth surface. In fact, the MATLAB analysis shows very localised and higher temperatures zones for the conventional insulator in comparison with the results of the textured insulator, where the area is more uniformly heated but with lower maximum values.

5 Surface conductance measurements

During a test using the RWDT, local surface conductance measurements were evaluated using a device built in according to IEC60507 standards [27]. The possible arrangement of this device is described by a conductance meter with two spherical probes. The probes were made of stainless-steel pins 5 mm in diameter with a

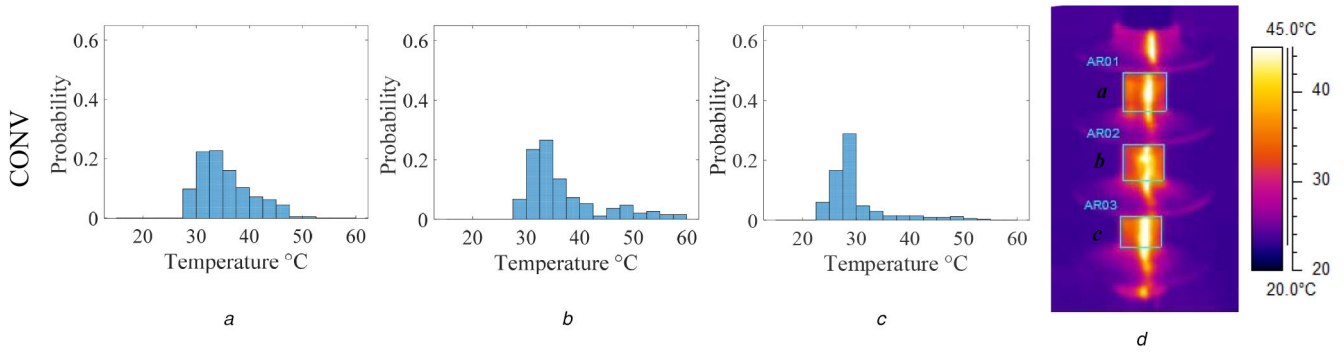

Fig. 12 *IR record and temperature probability over the trunk areas of conventional (CONV) design*
(a) Trunk 1, ***(b)*** Trunk 2, ***(c)*** Trunk 3, ***(d)*** IR record

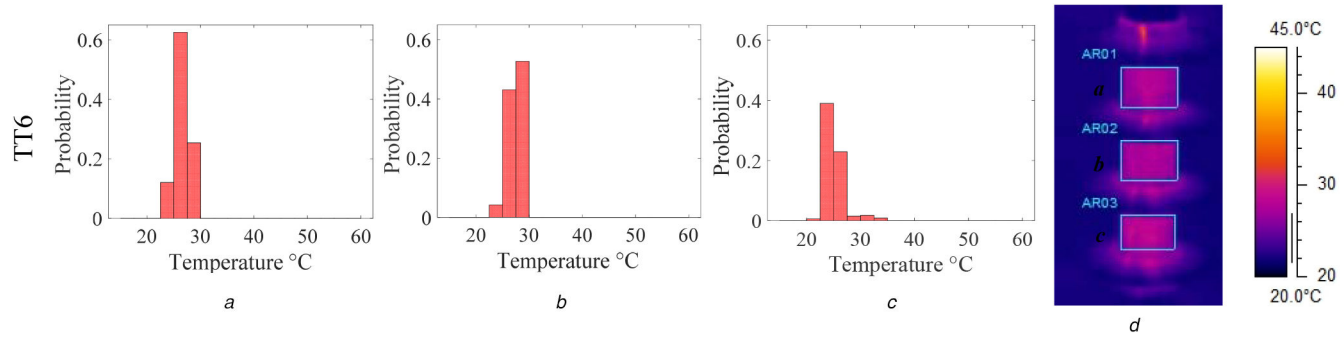

Fig. 13 *IR record and temperature probability over the trunk areas of textured (TT6) design*
(a) Trunk 1, ***(b)*** Trunk 2, ***(c)*** Trunk 3, ***(d)*** IR record

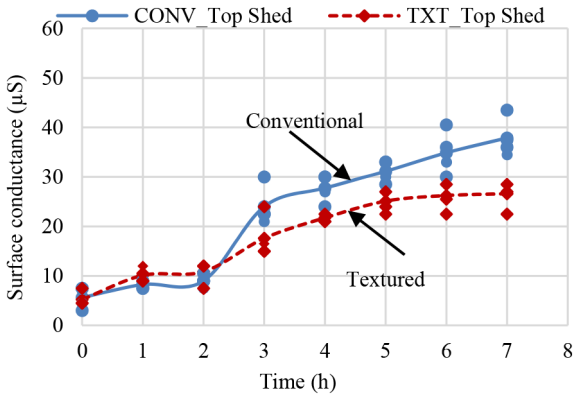

Fig. 14 *Average surface conductance measurements for the upper surfaces of the four sheds*

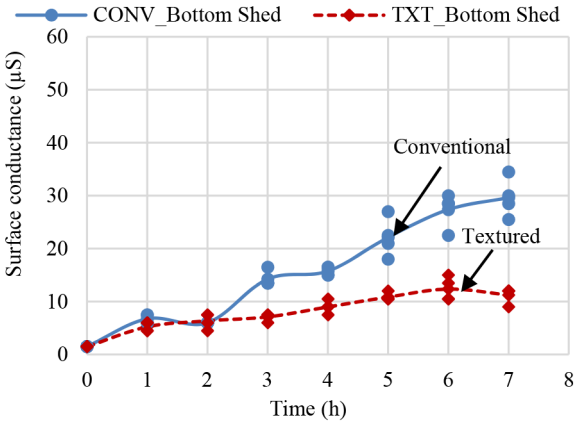

Fig. 15 *Average conductance measurements for the bottom surfaces of the four sheds*

distance of 14 mm between their centres. The pins were spring-loaded so they could be pushed by hand against the insulator surface. The spring force at full compression was around 9 N. The voltage source with a Zener-diode at 6.8 V supplied the current through a probe between the electrodes. The measuring meter offered different full-scale deflections at values of 50, 100 and 500 μA. The selector switch was used to determine the scale deflection suitable for the measurement ranges. The measurements of the pollution layer were carried out at different places on the insulator surfaces. The uniformity of the surface layer is attained when the difference between each measured value and their average, as a percentage, is limited to ±30%.

The probe was used to measure the conductance values on the insulator trunk, and top and bottom shed surfaces. The measurements were carried out for both insulator designs. The localised measurements were evaluated at selected times after the start of the test. This evaluation helped to identify and explain the trends of the conductance and its distribution on each insulator surface.

The average conductance measurements of the top and bottom sheds of tested insulators are described in Figs. 14 and 15, respectively. It is clear from the graphs that the textured profile had a lower increase during the test. The average surface conductance values of the upper shed surfaces for the textured insulator were significantly decreased by 22% in comparison with the conventional insulator. This can be clearly observed on the bottom shed curve (Fig. 15) where the increase of surface conductance values was marginal for the textured design and 46% decrease of surface conductance measurements attained compared with the conventional.

In the tested textured insulator, it should be highlighted that the sheds surfaces are not textured. Therefore, given inclined shed surfaces, the conductance of the upper surfaces of the conventional insulator is enhanced by a more uniform wetting of the surface compared to the textured insulator wetting which is affected by the trunk texture channelling water dripping from the hemispherical textures. For the bottom surfaces of the sheds, the difference is attributed to the higher power dissipation on the trunk of the conventional design causing more evaporation and condensation on the lower surfaces of the sheds.

A similar variation trend was also observed on the insulator trunk and a 42% reduction in surface conductance values was achieved, as can be clearly seen in Fig. 16.

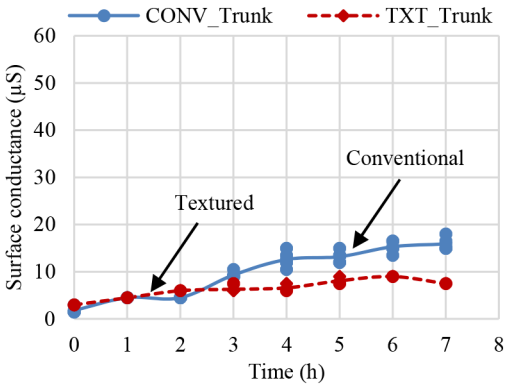

Fig. 16 *Average conductance measurements for the trunk of tested insulators*

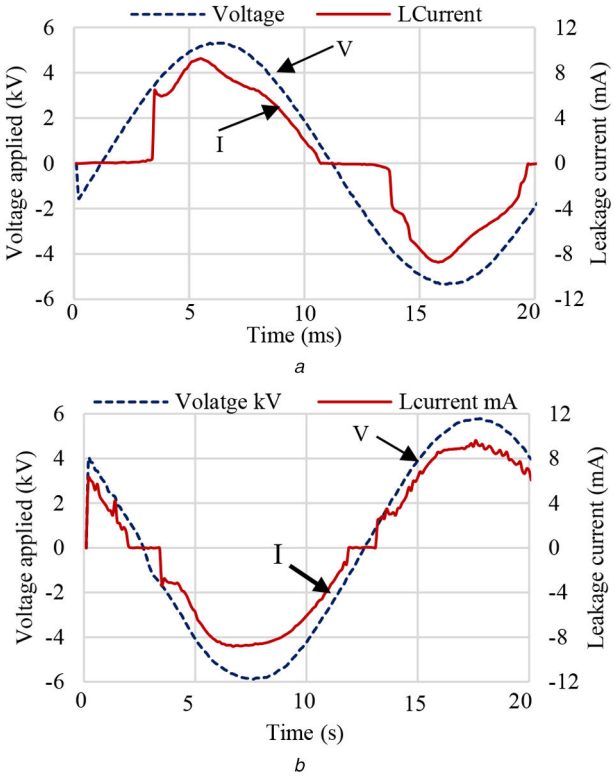

Fig. 17 *Leakage current and voltage applied waveforms*
(a) Conventional insulator, ***(b)*** Textured trunk insulator

6 AC test results

Several AC tests were performed on the two insulator designs. It has adopted the RWDT technique to focus on the insulator wetting surface performance (leakage current, power and energy dissipation) which allows a direct comparison between textured and non-textured insulators. The test is not aimed at measuring flashover performance or complying with standards.

6.1 Leakage current

Fig. 17 shows typical waveforms of applied voltage and leakage current for the conventional and textured insulators, measured during the 15th test cycle, 24 s after the start of the third period. It is clear from the two plots that discharge activity occurred on both surfaces. However, it was more intense on the conventional surface. The high resistive leakage current behaviour observed at initial energisation leads to drying of the surface and the formation of dry bands.

When the formation of dry band arcing occurs, this can be seen in the current waveform of the conventional insulator by the steps at 3.5 ms. This waveform is like that observed in [28]. In the case

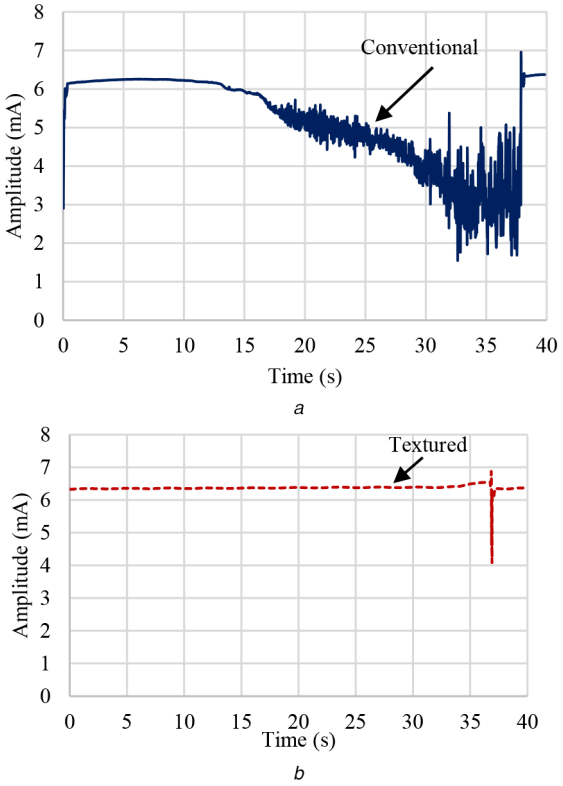

Fig. 18 *Typical RMS leakage current for tested insulators*
(a) Conventional insulator, ***(b)*** Textured trunk insulator

of a textured surface, the discharge activity is much lower, and a mostly conductive behaviour is observed.

6.2 RMS leakage current

Fig. 18 shows typical shapes of RMS leakage current measured for the tested insulators. As described earlier, each insulator was energised for a period of 40 s.

For the conventional insulator, the wet surface dried over time due to the dripping of water and Joule heating. Non-uniform discharge activity caused heavy arcing and further drying. This drying progression was accompanied by a fall in the leakage current magnitude reaching 3 mA at the end of the energisation period. For the textured insulator, a continuous thin conducting layer was maintained. Discharge activity was limited on the surface, and the magnitude of leakage current was slightly reduced. The key advantage of textured insulators is that of a multi-current path when wet pollution is present on the surface. This means that, as current flows and drives the path, it changes/jumps to another path that has lower impedance/resistance. Overall, this results in a highly distributed power consumption over the surface. However, the non-textured insulator tends to form focused currents paths which lead to dry bands and discharges; these cause tracking and erosion characterised by current/power values.

6.3 Power dissipation

Fig. 19 illustrates the average power dissipated on the surface of the test insulators during the 15th wheel revolution. It can be seen that the power dissipation for the conventional profile increases significantly until it reaches the initial peak value of 40 W after 20 s. However, with a textured profile, the trend of the shape is mostly constant with a lower value of power dissipation about 20 W. After the initial power peak on the conventional surface, the dissipated power decreases gradually and significant distortion is observed during this period. This distortion is caused by the increasing discharge activity occurring on the insulator surface. For textured insulator, the surface enables a significant reduction of current density associated to leakage current. The inclined plane test is an accelerated ageing test for material surfaces. Previous work in this area has been published in [29] and was shown that the multi-

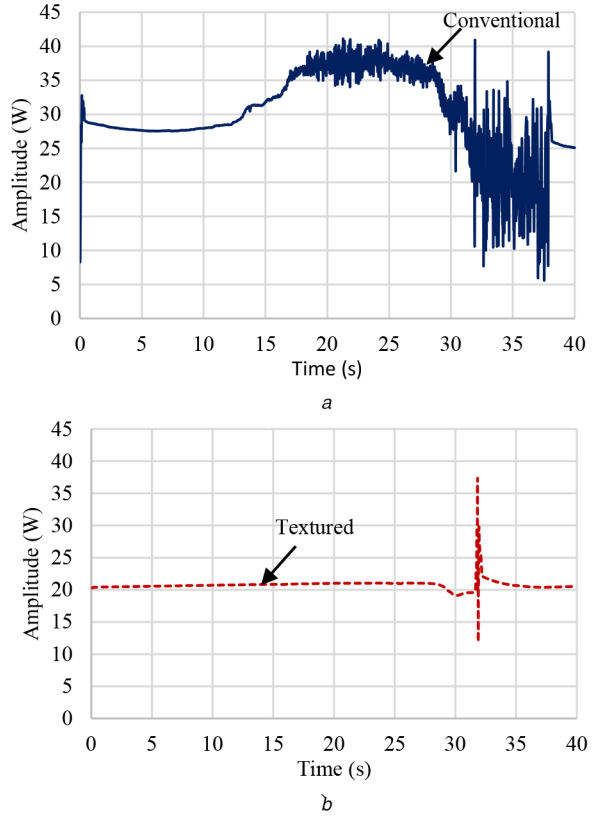

Fig. 19 *Average power dissipated for tested insulators*
(a) Conventional insulator, ***(b)*** Textured trunk insulator

current path in textured surfaces protects the surface from tracking and erosion damage compared with non-textured surface. In this way, we have shown that the textured surface will survive longer periods of testing. If the contamination level is very high, the erosion will happen, however after 10/15 years the texture dimples will show some erosion and bringing the situation like a conventional surface but not to failure. If same conditions would have been applied to a non-textured surface, the erosion would lead to the failure of the insulator. Therefore, the damage on the textured surface has always been less significant.

7 Conclusion

Two different designs of SiR insulators were manufactured in house and were tested using the RWDT. The RWDT facility and its construction was described. The software and the assembled hardware used to construct the wheel test system were extensively detailed. It was clear from the results that the higher temperature value was recorded on the conventional insulator. The visual capture revealed visible discharge activities and dry band arcing on the trunk surface of the conventional insulator which was not always observed for the textured insulator. Surface tracking and erosion defects were also seen on the conventional design at the end of the test. Moreover, the IR record and the spatial analysis using the MATLAB analysis routine confirmed that the higher stress zones were identified on the smooth surface of conventional insulator in comparison with the results of the textured insulator. In addition, a reduction of the surface conductance value index was achieved in the case of the textured insulator. For AC tests, the leakage current measurements showed that drying and discharge activity are greater for the conventional insulator compared with a textured insulator. The power dissipated by partial arcing in conventional design is expected to be more damaging than ohmic power loss for textured. This tendency suggested that the textured design reduces the hydrophobicity characteristics, and consequently, it can promote an increase in insulator's life expectancy and improve overall tracking and erosion performance.

8 References

[1] Hackam, R.: 'Outdoor HV composite polymeric insulators', *IEEE Trans. Dielectr. Electr. Insul.*, 1999, **6**, (5), pp. 557–585

[2] Kikuchi, T., Nishimura, S., Nagao, M., *et al.*: 'Survey on the use of non-ceramic composite insulators', *IEEE Trans. Dielectr. Electr. Insul.*, 1999, **6**, (5), pp. 548–556

[3] Reynders, J.P., Jandrell, I.R., Reynders, S.M.: 'Review of aging and recovery of silicone rubber insulation for outdoor use', *IEEE Trans. Dielectr. Electr. Insul.*, 1999, **6**, (5), pp. 620–631

[4] Gubanski, S.M., Dernfalk, A., Andersson, J., *et al.*: 'Diagnostic methods for outdoor polymeric insulators', *IEEE Trans. Dielectr. Electr. Insul.*, 2007, **14**, (5), pp. 1065–1080

[5] Cheng, L., Shao, S., Zhang, S., *et al.*: 'Research on the long-time operation performance of composite insulator shed hydrophobicity under hydrothermal conditions', *IET High Volt.*, 2017, **3**, (1), pp. 67–72

[6] Chakraborty, R., Reddy, S.B.: 'Performance of silicone rubber insulators under thermal and electrical stress', *IEEE Trans. Ind. Appl.*, 2017, **53**, (3), pp. 2446–2454

[7] Krzma, A.S., Albano, M., Haddad, A.: 'Flashover influence of fog rate on the characteristics of polluted silicone-rubber insulators'. 52nd Int. Universities Power Engineering Conf. (UPEC), Heraklion, Greece, December 2017, pp. 1–5

[8] Albano, M., Krzma, A.S., Waters, R.T., *et al.*: 'Artificial pollution layer characterization on conventional and textured silicone-rubber insulators'. The 19th Int. Symp. on High Voltage Engineering (ISH), Pilsen, Czech Republic, 2015

[9] Klüss, J.V., Hamilton, J.: 'Design of rotating wheel dip test system for standard tracking and erosion testing of polymeric insulators'. The 20th Int. Symp. on High Voltage Engineering (ISH), Buenos Aires, Argentina, August 2017

[10] Chakraborty, R., Subba Reddy, B.: 'Studies on high temperature vulcanized silicone rubber insulators under arid climatic aging', *IEEE Trans. Dielectr. Electr. Insul.*, 2017, **24**, (3), pp. 1751–1760

[11] Barsch, R., Jahn, H., Lambrecht, J., *et al.*: 'Test methods for polymeric insulating materials for outdoor HV insulation', *IEEE Trans. Dielectr. Electr. Insul.*, 1999, **6**, (5), pp. 668–675

[12] Li, S., Liang, X., Liu, Y., *et al.*: 'Investigation on tracking wheel test of large-diameter composite insulators under AC voltage', *IEEE Trans. Dielectr. Electr. Insul.*, 2017, **24**, (6), pp. 3522–3529

[13] Verma, A.R., Subba, R.B.: 'Understanding surface degradation on polymeric insulators using rotating wheel and dip test under DC stress', *IEEE Trans. Dielectr. Electr. Insul.*, 2018, **25**, (5), pp. 2029–2037

[14] Haddad, A., Waters, R., Griffiths, H., *et al.*: 'A new approach to anti-fog design for polymeric insulators', *IEEE Trans. Dielectr. Electr. Insul.*, 2010, **17**, (2), pp. 343–350

[15] Haddad, A., Waters, R.: 'Insulating structures'. UK Patent 2406225, 2003

[16] Wacker Chemie AG. Available at http://www.wacker.com, accessed June 2019

[17] Charalampidis, P.: 'Characterisation of textured insulators for overhead lines and substations'. PhD thesis, Cardiff University, 2012

[18] IEC 62730: 'HV polymeric insulators for indoor and outdoor use tracking and erosion testing by wheel test and 5 000h test', 2012

[19] Muncivi, A., Sarkar, P., Haddad, A.: 'Tracking wheel test facilities'. 44th Int. Universities Power Engineering Conf., Glasgow, UK, 2009, pp. 1–5

[20] 'LabVIEW user manual' (April 2003 Edition)

[21] Krzma, A.: 'Comparative laboratory performance characterisation of silicone rubber textured insulators'. PhD thesis, Cardiff University, 2016

[22] RS components: 'AEDB-9140 Series Data Sheet', January 2010

[23] Reading and writing TDMS files with NI LabVIEW. Available at http://www.ni.com/white-paper/3727/en/#toc3, accessed 25 February 2019

[24] Grasaesom, J., Thaong-om, S., Payakcho, W., *et al.*: 'Ageing deterioration of silicone rubber polymer insulator under salt water dip wheel test', *J. World Acad. Sci. Eng. Technol.*, 2011, **56**, pp. 211–217

[25] Heger, G., Vermeulen, H., Holtzhausen, J.: 'A comparative study of insulator materials exposed to high voltage AC and DC surface discharges', *IEEE Trans. Dielectr. Electr. Insul.*, 2010, **17**, (2), pp. 513–520

[26] Krzma, A.S., Albano, M., Waters, R.T., *et al.*: 'Comparative performance of 11 kV silicone rubber polymeric insulators with HVAC and HVDC excitations using the rotating wheel dip test'. The 19th Int. Symp. on High Voltage Engineering (ISH), Pilsen, Czech Republic, 2015

[27] IEC 60507: 'Artificial pollution tests on high-voltage ceramic and glass insulators to be used on a.c. systems', 3rd edition, 2013

[28] Marungsri, B., Shinokubo, H., Matsuoka, R.: 'Effect of specimen configuration on deterioration of silicone rubber for polymer insulators in slat fog aging test', *IEEE Trans. Dielectr. Electr. Insul.*, 2006, **13**, (2), pp. 129–138

[29] Waters, R.T., Haddad, A., Griffiths, H, *et al.*: 'Dry-band discharges on polluted silicone rubber insulation: control and characterization', *IEEE Trans. Dielectr. Electr. Insul.*, 2011, **18**, (6), pp. 1995–2003